Research Article Vol. 32, No. 1 / 1 Jan 2024 / Optics Express 179
Optics EXPRESS

Experimental study of modified Tavis-Cummings model with directly-coupled superconducting artificial atoms

JIAN-YONG ZHOU,[1,†] SI-LU ZHAO,[2,3,†] YA YANG,[1] SHI XIAO,[1,2] D. HE,[1] WEI NIE,[4] YING HU,[1] JING LU,[1] LE-MAN KUANG,[1] YU-XI LIU,[5] MING-TANG DENG,[6] DONG-NING ZHENG,[2,3] ZHONG-CHENG XIANG,[2,7] LAN ZHOU,[1,8] AND Z. H. PENG[1,9]

[1]*Key Laboratory of Low-Dimensional Quantum Structures and Quantum Control of Ministry of Education, Department of Physics and Synergetic Innovation Center for Quantum Effects and Applications, Hunan Normal University, Changsha 410081, China*
[2]*Institute of Physics, Chinese Academy of Sciences, Beijing 100190, China*
[3]*School of Physical Sciences, University of Chinese Academy of Sciences, Beijing 100049, China*
[4]*Center for Joint Quantum Studies and Department of Physics, School of Science, Tianjin University, Tianjin 300350, China*
[5]*School of Integrated Circuits, Tsinghua University, Beijing 100084, China*
[6]*Institute for Quantum Information State Key Laboratory of High Performance Computing, Changsha 410081, China*
[7]*zcxiang@iphy.ac.cn*
[8]*zhoulan@hunnu.edu.cn*
[9]*zhihui.peng@hunnu.edu.cn*
[†]These authors contributed equally to this work.

Abstract: The Tavis-Cummings model is intensively investigated in quantum optics and has important applications in generation of multi-atom entanglement. Here, we employ a superconducting circuit quantum electrodynamic system to study a modified Tavis-Cummings model with directly-coupled atoms. In our device, three superconducting artificial atoms are arranged in a chain with direct coupling through fixed capacitors and strongly coupled to a transmission line resonator. By performing transmission spectrum measurements, we observe different anticrossing structures when one or two qubits are resonantly coupled to the resonator. In the case of the two-qubit Tavis-Cummings model without qubit-qubit interaction, we observe two dips at the resonance point of the anticrossing. The splitting of these dips is determined by $\Delta\lambda = 2\sqrt{g_1^2 + g_3^2}$, where g_1 and g_3 are the coupling strengths between Qubit 1 and the resonator, and Qubit 3 and the resonator, respectively. The direct coupling J_{12} between the two qubits results in three dressed states in the two-qubit Tavis-Cummings model at the frequency resonance point, leading to three dips in the transmission spectrum. In this case, the distance between the two farthest and asymmetrical dips, arising from the energy level splitting, is larger than in the previous case. The frequency interval between these two dips is determined by the difference in eigenvalues ($\Delta\lambda = \varepsilon_{1+} - \varepsilon_{1-}$), obtained through numerical calculations. What we believe as novel and intriguing experimental results may potentially advance quantum optics experiments, providing valuable insights for future research.

1. Introduction

Generalizing a single two-level atom Rabi system [1], which describes the interaction of a two-level atom and a single-mode cavity, to N atoms case leads to the well-known Dicke model [2]. When the cavity and the atoms in the Dicke model are nearly resonant, and the system

#509250 https://doi.org/10.1364/OE.509250
Journal © 2024 Received 13 Oct 2023; revised 29 Nov 2023; accepted 2 Dec 2023; published 18 Dec 2023

Optics EXPRESS

remains in a weak or strong coupling regime, the Tavis-Cummings (TC) model is derived by employing the rotating wave approximation (RWA) [3]. Enhancing the collective coupling strength with an increasing number of atoms, following a relationship of $G = g\sqrt{N}$ in Ref. [3] was predicted. Cavity quantum electrodynamics (QED) [4–7] has achieved considerable attention in the study of atom-cavity interactions, particularly in solid-state semiconductor systems [8–12], superconducting quantum circuits [13–17], and quantum dot systems [9]. Over the years, the experimental observations of vacuum Rabi splitting [8–12,18–20] and vacuum Rabi oscillations [21–23], predominantly manifested in the energy level anticrossing phenomenon between a qubit and a resonator, which has provided compelling evidence of strong light-atom coupling.

Circuit quantum electrodynamics (Circuit QED), serving as an excellent experimental platform for superconducting quantum systems, has enabled the realization of the standard Jaynes-Cummings (JC) model in cavity QED through the strong coupling of superconducting artificial atoms and a transmission line resonator [24]. An experiment of strong coupling between a single photon and a superconducting qubit was carried out with a circuit QED system and an anticrossing phenomena was observed [14]. Furthermore, when one or two photons are strongly coupled to artificial atoms, the energy level splitting experimental results of the first $|1\pm\rangle$ and second $|2\pm\rangle$ doublet states confirm the nonlinearity of the JC model [25]. Vacuum Rabi splitting, resulting from the coupling of a multi-level atom to a transmission line resonator, gives rise to doublets, and the observed sector-shaped anticrossing structures generated by multiphoton transitions under high driving power follows a $\sqrt{n}$ pattern in the JC ladder [26].

The TC model was extensively explored based on circuit QED and waveguide QED. In multi-qubit TC models, the creation of maximum Greenberger-Horne-Zeilinger entangled states is deterministically allowed [27], and the strong coupling between the cavity and qubits leads to the suppression of qubit linewidth [28]. The collective effects of multiple qubits coupled to a cavity lead to a dispersive frequency shift of the cavity, resulting in an ensemble's AC Stark shift [29]. In addition, the effect enables the investigation of quantum critical behavior based on superconducting circuits [30]. Subsequently, the TC model was studied with an impressive number of 4300 superconducting qubits in an experiment, and the collective effects of the qubits have greatly facilitated the significant dispersive frequency shift of the cavity [31].

There are some research on energy level anticrossing using circuit QED system. Considering qubits without interaction, the JC and TC models of strong coupling between them and the cavity field, the experimental energy level splittings of these different models revealed a dispersion of collective atomic coupling strength following a $\sqrt{N}$ relationship in Ref. [32]. Two qubits with adjustable effective distance are coupled to a one-dimensional coplanar waveguide, and the super- and sub-radiant states are generated in the case of decoupling between the two qubits. However, when the virtual photon induces indirect coupling between two qubits, the phenomenon of anticrossing of the qubit energy levels occurs, and the super- and sub-radiant states disappears [33]. Two transmon qubits are coupled to a one-dimensional waveguide, and interatomic interactions mediated by virtual photons result in a large collective Lamb shift. This is reflected in the observation of obvious anticrossing between the two qubits, and the minimum size of the resonance point separation reaches twice the transition line width [15]. Theoreticians predicted that the spacing and depth of the two dips of the output spectrum determined by the modified TC model are influenced by the number of atoms and the coupling strength between them [34].

Our experiment studied the modified TC model with three tunable Xmon qubits (artificial atoms) arranged in a chain with direct coupling through a fixed capacitor and strongly coupled to a one-dimensional transmission line resonator (cavity). In Sec. 2, we presented the system's theoretical model and circuit diagram and conducted characterizations of the coupled system. In Sec. 3, we measured and analyzed the energy level splittings of the system with or without direct interactions between the atoms, respectively. Finally, in Sec. 4, we gave the conclusion.

Optics EXPRESS

2. Theoretic model and sample characterization

As illustrated in Fig. 1, the device comprises three Xmon qubits, denoted as qubits 1, 2, and 3, respectively, that are capacitively coupled to a single-mode cavity simultaneously. Meanwhile, the three qubits are strongly coupled to a one-dimensional transmission line (open space) utilized for spectrum measurement in the experiment (not illustrated). In the experiment, we studied the two-qubit TC model without or with direct coupling between the two qubits by selecting qubits 1 and 3 or 1 and 2 are simultaneously resonant to the cavity, respectively, while keeping the last qubit far detuned from the cavity. The Hamiltonian describes this system under the RWA, denoted as

$$H = \hbar\omega_r a^\dagger a + \sum_{i=1}^{3} \xi_i \hbar \left(\frac{1}{2}\omega_i \sigma_{zi} + g_i a^\dagger \sigma_i^- + g_i a \sigma_i^+ \right) + \xi_2 \hbar J_{12} \left(\sigma_1^+ \sigma_2^- + \sigma_2^+ \sigma_1^- \right). \tag{1}$$

Here, σ_{zi} and $\sigma_i^+ = |e\rangle\langle g|$ ($\sigma_i^- = |g\rangle\langle e|$) represent the Pauli operators and raising (lowering) operators of qubit i ($i = 1, 2, 3$), where $|e\rangle$ and $|g\rangle$ correspond to the excited state and ground state of the qubit i, respectively. The photon creation (annihilation) operator of the resonator is denoted by $a^\dagger$ (a). The parameter ξ_i is used to split Eq. (1) into two-qubit TC model of the two distinct cases, where $\xi_1 = 1$, $\xi_2 = 0$, and $\xi_3 = 1$ ($\xi_1 = 1$, $\xi_2 = 1$, and $\xi_3 = 0$) represents Case 1 (Case 2).

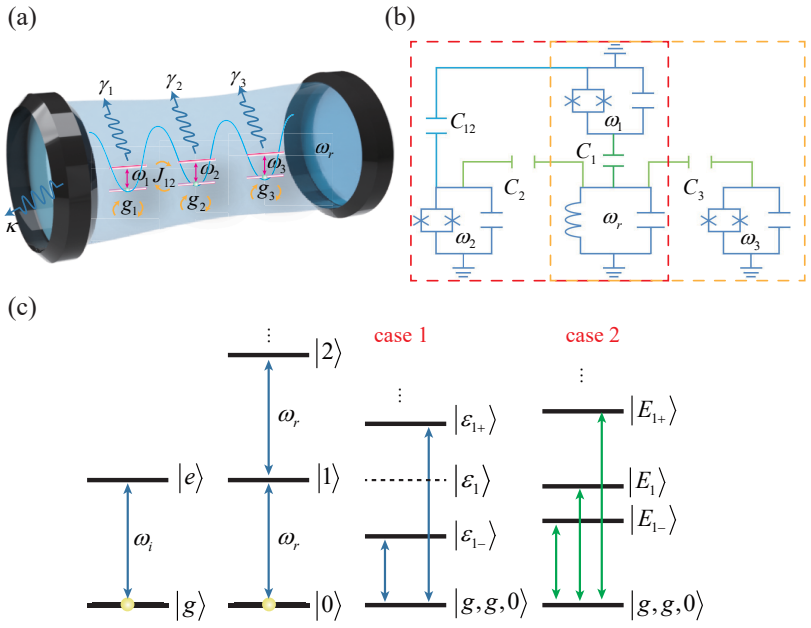

Fig. 1. (a) Theoretical model. For brevity, this figure illustrates both two-qubit TC models in Cases 1 ($\xi_1 = 1$, $\xi_2 = 0$, $\xi_3 = 1$) and 2 ($\xi_1 = 1$, $\xi_2 = 1$, $\xi_3 = 0$). Decay rate of resonator is $\kappa/2\pi = 22$ MHz, and relaxation rates of Qubits 1, 2, and 3 are $\gamma_1/2\pi = 51$ MHz, $\gamma_2/2\pi = 43$ MHz, $\gamma_3/2\pi = 41$ MHz, respectively. (b) Simplified circuit model of two-qubit TC system is demonstrated. Red and orange dotted lines represent Cases 1 and 2, respectively. (c) Simplified diagrams illustrating energy level distribution. State $|0\rangle$ ($|1\rangle$, $|2\rangle$) corresponds to the photon number state of the resonator. Applying appropriate driving can induce transitions in the system. Blue and green double-headed arrows indicate transitions in Cases 1 and 2, respectively.

Optics EXPRESS

In Fig. 1(a), the three qubits, with transition frequencies ω_1, ω_2 and ω_3, respectively, are coupled to a cavity with resonance frequency ω_r. The coupling strengths between the cavity and qubit i are denoted by g_i. Qubits 1 and 2 are directly coupled to each other with a coupling strength of J_{12}. However, there is no direct coupling between qubits 1 and 3. Therefore, the following two cases are taken into account: 1) $\xi_1 = 1$, $\xi_2 = 0$, $\xi_3 = 1$, where is the original two-qubit TC model case and corresponds to only qubits 1 and 3 are simultaneously resonant to the cavity without direct coupling between the two qubits. 2) $\xi_1 = 1$, $\xi_2 = 1$, $\xi_3 = 0$, where is the modified two-qubit TC model case and corresponds to only Qubits 1 and 2 are simultaneously resonant to the cavity with direct coupling between the two qubits.

The simplified circuit model is presented in Fig. 1(b). We realized nearest-neighbor coupling between qubits 1 and 2 through the capacitor C_{12} and three qubits are strong coupling to the transmission line resonator through the capacitors C_1, C_2 and C_3, respectively. On-chip control lines could independently tune the transition frequency of each qubit. Therefore, we achieved Cases 1 or 2 by adjusting the transition frequency of qubits 2 or 3 to be below $2\pi \times 4$ GHz, which is far detuning from the frequencies of the cavity and the other two qubits. In Cases 1 and 2, we can implement two TC models to study the influence of direct coupling between two qubits on energy level anticrossing.

To predict the frequency intervals of energy level splitting in the two cases from a theoretical point of view, we first analyze the eigensystems in the two cases. Clearly, for Case 1 of the Hamiltonian in Eq. (1), the conserved quantity of the two-qubit TC model is $N = a^\dagger a + \sigma_{z1}/2 + \sigma_{z3}/2$. When the conserved quantity is truncated to the single excitation case ($N = 1$), the basis is reduced to the three states $|1, g, g\rangle$, $|0, e, g\rangle$, and $|0, g, e\rangle$. The state $|0, g, g\rangle$ represents both qubits being in the ground state with no photons in the resonator. For convenience, we consider the case of $\omega = \omega_r = \omega_1 = \omega_3$. The Hamiltonian of Case 1 can be written as a matrix:

$$H = \begin{pmatrix} \omega & g_3 & g_1 \\ g_3 & \omega & 0 \\ g_1 & 0 & \omega \end{pmatrix}. \tag{2}$$

Its corresponding eigenvalues are

$$\begin{aligned} \varepsilon_{1-} &= \omega - \bar{g}, \\ \varepsilon_1 &= \omega, \\ \varepsilon_{1+} &= \omega + \bar{g}, \end{aligned} \tag{3}$$

where we adopted the following definition

$$\bar{g}^2 = \left(g_1^2 + g_3^2\right), \tag{4}$$

and the eigenvectors after normalization are

$$\begin{aligned} |\varepsilon_{1-}\rangle &= -\frac{1}{\sqrt{2}}|1, g, g\rangle + \frac{g_3}{\sqrt{2}\bar{g}}|0, g, e\rangle + \frac{g_1}{\sqrt{2}\bar{g}}|0, e, g\rangle, \\ |\varepsilon_1\rangle &= -\frac{g_1}{\bar{g}}|0, g, e\rangle + \frac{g_3}{\bar{g}}|0, e, g\rangle, \\ |\varepsilon_{1+}\rangle &= \frac{1}{\sqrt{2}}|1, g, g\rangle + \frac{g_3}{\sqrt{2}\bar{g}}|0, g, e\rangle + \frac{g_1}{\sqrt{2}\bar{g}}|0, e, g\rangle. \end{aligned} \tag{5}$$

Because an analytical expression for the eigensystem cannot be obtained in Case 2, numerical methods are employed to solve for the eigenvalues and eigenvectors. Figure 1(c) illustrates the related transitions of the TC models in Cases 1 and 2, respectively. We introduce two states

Optics EXPRESS

$|B\rangle = \frac{g_1}{g}|e,g\rangle + \frac{g_3}{g}|g,e\rangle$ and $|D\rangle = \frac{g_3}{g}|e,g\rangle - \frac{g_1}{g}|g,e\rangle$ that are only related to the atomic states. In Case 1, the cavity field is only coupled to state $|B\rangle$ and is decoupled from state $|D\rangle$, which causes the the eigenstate $|\varepsilon_1\rangle$ not to exist at the resonance point ω. Therefore, the system exhibits only two effective eigenstates $|\varepsilon_{1-}\rangle$ and $|\varepsilon_{1+}\rangle$. In case 2, the interaction between the qubits J_{12} induces the coupling of states $|B\rangle$ and $|D\rangle$, resulting in a new eigenstate $|E_1\rangle$. All three eigenstates incorporate the single-photon state $|1\rangle$ of the cavity, therefore, the system's energy spectrum features three eigenvalues at the cavity frequency degeneracy ω.

Our experiment is carried out in a dilution refrigerator at a base temperature of around 30 mK. From the transmission measurement, the fundamental frequency of the resonator $\omega_r/2\pi \approx 4.285$ GHz with decay rate $\kappa/2\pi \approx 22$ MHz when all qubits are far detuned from the resonator mode. As illustrated in Fig. 2, a two-dimensional transmission plot of the transmission amplitude through the transmission line is measured in the frequency range of 4-5.2 GHz with the magnetic flux bias $\delta\Phi_1$ from -400 to 400 mΦ_0 with a vector network analyzer (VNA), where Φ_0 is the flux quantum $\Phi_0 = h/2e$. From the data, we extracted the maximum Josephson energy $E_{j1,\max}/h \approx 321.3$ GHz and the charging energy $E_{c1} \approx 10$ MHz of qubit 1. We performed similar characterizations for qubits 2 and 3 (not indicated in text) and extracted maximum Josephson energies $E_{j2,\max}/h \approx 305.4$ GHz and $E_{j3,\max}/h \approx 322.6$ GHz, charging energies $E_{c2} \approx 11$ MHz and $E_{c3} \approx 11$ MHz, respectively. Furthermore, the maximum transition frequencies of Qubits 2 and 3 are $\omega_{2,\max} \approx \omega_{3,\max} \approx 2\pi \times 5.22$ GHz.

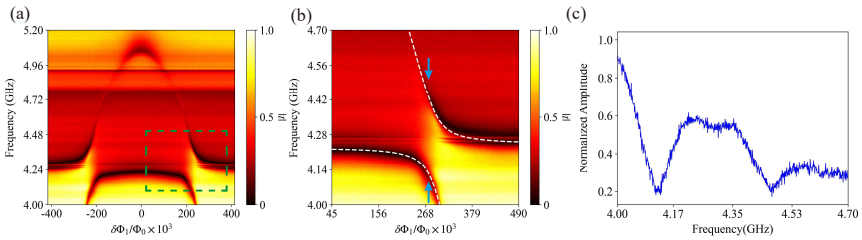

Fig. 2. (a) Transmission spectrum through qubit 1. Transmission amplitude coefficient $|t|$ as function of magnetic flux bias $\delta\Phi_1$ and probing frequency. Transitions $|g\rangle \leftrightarrow |e\rangle$ are revealed as sharp dips. Maximum transition frequency of qubit $\omega_{1,\max}/2\pi = 5.06$ GHz at $\delta\Phi_1 = 0$. There are two anticrossings due to coupling to resonator around $\delta\Phi_1 \sim \pm 200 \times 10^{-3}\Phi_0$. (b) Anticrossing in spectroscopy of qubit magnified with dashed green rectangle range in Fig. 2(a). White dashed curve is theoretical calculations of energy levels. (c) Splitting at positions indicated by arrows, and coupling strength between qubit and resonator is extracted as $g_1 = 2\pi \times 150$ MHz.

In Fig. 2(b), it indicates that qubit 1 is resonant with the fundamental mode of the resonator when the biased flux $\delta\Phi_1 \approx 276$ mΦ_0. At this degeneracy point, the anticrossing in the energy levels occurs, leading to a split energy spectrum with two curves. We extracted the coupling strength $g_1/2\pi = 150$ MHz between qubit 1 and the resonator mode from the fitting of the anticrossing. Similarly, the coupling strengths between qubit 2 and the resonator mode, and qubit 3 and the resonator mode, are $g_2 \approx g_3 = 2\pi \times 90$ MHz, respectively. The system works in a regime of strong coupling because the minimum of (g_1, g_2, g_3, J_{12}) is larger than the maximum of $(\kappa, \gamma_1, \gamma_2, \gamma_3)$.

3. Splitting of anticrossing in the TC model

After performing basic characterizations on the device, we studied the anticrossing in the energy levels of the two-qubit TC model system for Cases 1 and 2, respectively. First, we measured the anticrossing of the coupled system works in Case 1 where qubits 1 and 3 were not directly coupled. Here, we kept Qubit 3 at degeneracy ($\omega_3 = \omega_r$) and observed the one-photon one-qubit

Optics EXPRESS

doublet (see left of Fig. 3(a)). Here, qubit 2 remained far detuned from the resonator mode for Case 1 measurement. Qubit 1 is then tuned through the qubit-resonator coupled states from lower to higher values of biased flux $\delta\Phi_1$. When both qubits and the resonator are exactly in resonance at the positions ($\delta\Phi_1 \approx 278\,\mathrm{m}\Phi_0$) indicted by arrows in Fig. 3(a), we observed two distinct dips presented in Fig. 3(b) with a frequency interval between them $\sim 2\pi \times 358$ MHz. The two dips corresponded to the doublet $|\varepsilon_{1-}\rangle$ and $|\varepsilon_{1+}\rangle$ with eigenenergies $\hbar(\omega_r - \Delta\lambda/2)$ and $\hbar(\omega_r + \Delta\lambda/2)$, respectively.

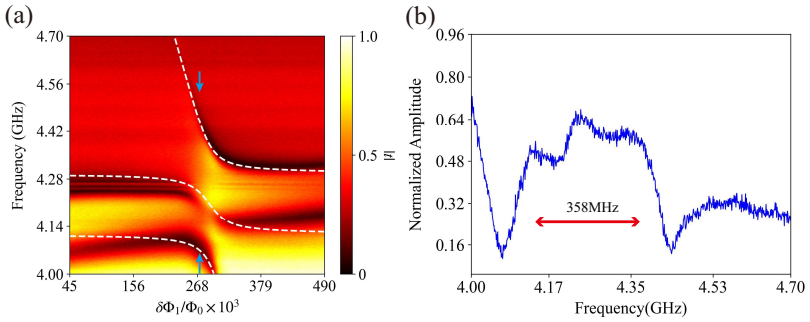

Fig. 3. (a) Resonator transmission spectrum reveals the coupled system energy level anticrossing in Case 1. Here, we keep qubit 3 at the degeneracy ($\omega_3 = \omega_r$) and vary the flux bias of qubit 1. (b) Splitting at positions is indicated by arrows in (a). Frequency interval between two dips is around $\sim 2\pi \times 358$ MHz, indicating splitting of energy levels.

We theoretically calculated the energy levels by diagonalizing the Hamiltonian in Eq. (1) with the extracted experimental parameters and presented it as the dashed curve in Fig. 3(a). There was consistency in the experimental and theoretical results. In two sides of Fig. 3(a), it is evident that there are three dips corresponding to three dressed states of the coupled system when qubit 1 is not biased at degeneracy. According to Eq. (5), when the resonator and the qubits degenerate, the system's energy levels split into two dressed states, resulting in two symmetric dips with equal depth. It is consistent with the results presented in Fig. 3(b). The symmetric nature of the dips around ω_r can be inferred from the relationship $(\varepsilon_{1+} + \varepsilon_{1-})/2 = \omega_r$. The difference determines the splitting interval

$$\Delta\lambda = \varepsilon_{1+} - \varepsilon_{1-} = 2\sqrt{\left(g_1^2 + g_3^2\right)} = 2\pi \times 350\ \mathrm{MHz} \tag{6}$$

between the two effective eigenvalues. Notably, it agrees well with the experimental value $2\pi \times 358$ MHz.

Next, we carried out measurements for Case 2, where Qubits 1 and 2 were directly coupled with a fixed capacitor C_{12} in Fig. 1. In Fig. 4, we fixed the transition frequency of qubit 1 around 4.53 GHz and measured the transmission spectrum through qubit 2 in a frequency range from 4.2 GHz to 4.8 GHz. The dashed curve is the theoretical calculation by diagonalizing the system Hamiltonian, and we obtained the coupling strength $J_{12} = 2\pi \times 90$ MHz between qubits 1 and 2.

As presented in Fig. 5(a), the direct interaction between the two qubits affects the anticrossing in the spectroscopy of qubits 1 and 2, which are simultaneously resonant to the resonator mode. Here, we kept qubit 2 at degeneracy and qubit 3 significantly detuned from the resonator mode for the entire Case 2 measurement. The energy level splitting in the spectroscopy was no longer symmetrical, and there was a shifted spectral line at degeneracy. Extracting the experimental data at $\delta\Phi_1 \approx 278\,\mathrm{m}\Phi_0$ from Fig. 5(a), we observed that the frequency splitting size between the upper and lower, middle and upper, and middle and lower anticrossing levels were approximately

Optics EXPRESS

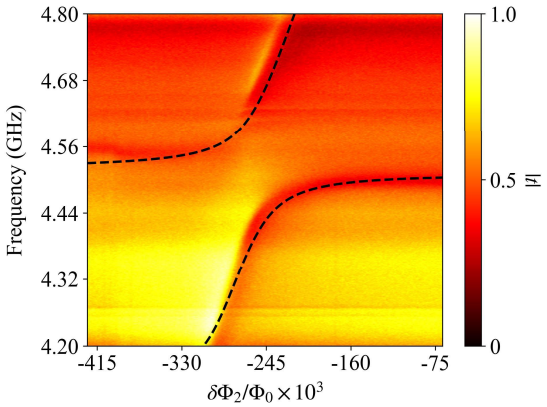

Fig. 4. Anticrossing in spectroscopy of qubit 2 where qubit 1 is biased at $\omega_1/2\pi = 4.53$ GHz. Dashed lines are theoretical calculations of energy levels, and extracted direct coupling strength between two qubits is $J_{12}/2\pi = 90$ MHz.

380 MHz, 260 MHz, and 120 MHz, respectively, as depicted in Fig. 5(b). Introducing coupling between the two qubits enhanced the separation between the two dips on the left and right sides.

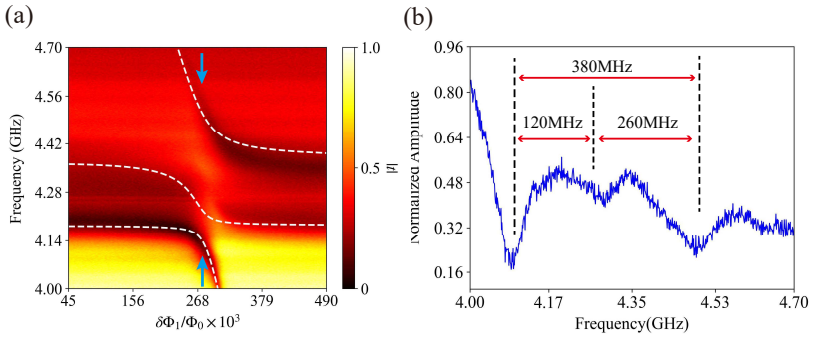

Fig. 5. (a) Resonator transmission spectrum reveals the coupled system energy level anticrossing in Case 2. Dashed curve is theoretical calculation of energy levels. Here, we keep qubit 2 at the degeneracy ($\omega_2 = \omega_r$) and vary the flux bias of qubit 1. (b) Two-dimensional representation indicates three dips with different depths and asymmetry.

The dashed curve in Fig. 5(a) is the theoretical simulation by diagonalizing the system Hamiltonian. According to the theory, three dips are expected to appear at the system's resonance point ω because there is a single-photon state $|1\rangle$ of the cavity in the eigenstate $|E_1\rangle$, as shown in Case 2 of Fig. 1(c). From Fig. 5(b), we can observe that, in addition to the two deeper dips on the left and right sides, there is also a relatively shallower dip in the middle. By performing numerical calculations, the intervals between the two asymmetrically separated dips on the left and right sides, right and middle side, and middle and left side were expressed as $\Delta\lambda_1 = E_{1+} - E_{1-} \approx 373$ MHz, $\Delta\lambda_2 = E_{1+} - E_1 \approx 295$ MHz, and $\Delta\lambda_3 = E_1 - E_{1-} \approx 77$ MHz, respectively. Remarkably, the experimental result of interval between the left dip and right dip is in good agreement with the theoretical calculation. However, the deviation between theory and experiment for intervals between the middle and right side, middle and left side may come from the uncertain position of the middle dip which is affected by background of measurement setup.

By comparing the theoretical results of Cases 1 and 2, we observed that the cavity field is only coupled to state $|B\rangle$ and has no interaction with state $|D\rangle$ in Case 1. Consequently, only two

Optics EXPRESS

energy level splittings occurred at this point, resulting in two symmetric dips about the resonant point, which aligned with the observed experimental results for Case 1. In Case 2, the qubit-qubit interaction allowed state $|B\rangle$ and state $|D\rangle$ are coupled, resulting in eigenstate $|E_1\rangle$. This led to three energy level splittings at the resonant point, manifesting as three asymmetric dips. The experimental results revealed the presence of three clear dips. The interaction between the qubits in Case 2 results in a larger energy level splitting scale compared to Case 1, which is evident from the wider frequency interval between the two farthest dips in Fig. 5(a) compared to the dips in Fig. 3(a).

4. Conclusion

In conclusion, we studied the energy level anticrossing in the TC models, where two qubits were coupled to a single-mode cavity in two cases. In the case of the two-qubit TC model without interaction between the qubits, we observed two dips with equal depth and symmetry about the degeneracy point. However, if there was interaction between the qubits, we observed an increase in the distance between the farthest two dips, and the symmetry of the dips was no longer maintained. In Cases 1 and 2, the frequency interval between the farthest two dips at the resonance point was found to be equal to the difference between their respective maximum and minimum eigenvalues, $\Delta\lambda = \varepsilon_{1+} - \varepsilon_{1-}$. This observation provides new insights on TC models and enriches experimental research on quantum optics based on superconducting quantum circuits.

Funding. National Natural Science Foundation of China (Grant No. 11935006, Grant No. 11975095, Grant No. 12061131011, Grant No. 12074117, Grant No. 1217050862, Grant No. 12247105, Grant No. 61833010); Science Fund for Distinguished Young Scholars of Hunan Province (Grant No. 2021JJ10043); Innovation Program for Quantum Science and Technology (No. 2-6).

Disclosures. The authors declare no conflicts of interest.

Data Availability. Data underlying the results presented in this paper are not publicly available at this time but may be obtained from the authors upon reasonable request.

References

1. I. I. Rabi, "Space quantization in a gyrating magnetic field," Phys. Rev. **51**(8), 652–654 (1937).
2. R. H. Dicke, "Coherence in Spontaneous Radiation Processes," Phys. Rev. **93**(1), 99–110 (1954).
3. M. Tavis and F. W. Cummings, "Exact Solution for an *N*-Molecule–Radiation-Field Hamiltonian," Phys. Rev. **170**(2), 379–384 (1968).
4. J. M. Raimond, M. Brune, and S. Haroche, "Manipulating quantum entanglement with atoms and photons in a cavity," Rev. Mod. Phys. **73**(3), 565–582 (2001).
5. R. Miller, T. E. Northup, K. M. Birnbaum, *et al.*, "Trapped atoms in cavity QED: coupling quantized light and matter," J. Phys. B **38**(9), S551–S565 (2005).
6. H. Walther, B. T. H. Varcoe, B.-G. Englert, *et al.*, "Cavity quantum electrodynamics," Rep. Prog. Phys. **69**(5), 1325–1382 (2006).
7. H. Mabuchi and A. C. Doherty, "Cavity quantum electrodynamics: Coherence in context," Science **298**(5597), 1372–1377 (2002).
8. J. P. Reithmaier, G. Sek, A. Löffler, *et al.*, "Strong coupling in a single quantum dot-semiconductor microcavity system," Nature **432**(7014), 197–200 (2004).
9. T. Yoshie, A. Scherer, J. Hendrickson, *et al.*, "Vacuum Rabi splitting with a single quantum dot in a photonic crystal nanocavity," Nature **432**(7014), 200–203 (2004).
10. E. Peter, P. Senellart, D. Martrou, *et al.*, "Exciton-photon strong-coupling regime for a single quantum dot embedded in a microcavity," Phys. Rev. Lett. **95**(6), 067401 (2005).
11. K. Hennessy, A. Badolato, M. Winger, *et al.*, "Quantum nature of a strongly coupled single quantum dot-cavity system," Nature **445**(7130), 896–899 (2007).
12. D. Englund, A. Faraon, I. Fushman, *et al.*, "Controlling cavity reflectivity with a single quantum dot," Nature **450**(7171), 857–861 (2007).
13. I. Chiorescu, P. Bertet, K. Semba, *et al.*, "Coherent dynamics of a flux qubit coupled to a harmonic oscillator," Nature **431**(7005), 159–162 (2004).
14. A. Wallraff, D. I. Schuster, A Blais, *et al.*, "Strong coupling of a single photon to a superconducting qubit using circuit quantum electrodynamics," Nature **431**(7005), 162–167 (2004).
15. P. Y. Wen, K.-T. Lin, A. F. Kockum, *et al.*, "Large Collective Lamb Shift of Two Distant Superconducting Artificial Atoms," Phys. Rev. Lett. **123**(23), 233602 (2019).

Optics EXPRESS

16. R. Dassonneville, T. Ramos, V. Milchakov, *et al.*, "Fast high-fidelity quantum nondemolition qubit readout via a nonperturbative Cross-Kerr coupling," Phys. Rev. X **10**(1), 011045 (2020).
17. S. Cao, B. Wu, F. Chen, *et al.*, "Generation of genuine entanglement up to 51 superconducting qubits," Nature **619**(7971), 738–742 (2023).
18. Y.-F. Zhu, D. J. Gauthier, S. E. Morin, *et al.*, "Vacuum Rabi splitting as a feature of linear-dispersion theory: Analysis and experimental observations," Phys. Rev. Lett. **64**(1), 2499–2502 (1990).
19. R. J. Thompson, G. Rempe, and H. J. Kimble, "Observation of normal-mode splitting for an atom in an optical cavity," Phys. Rev. Lett. **68**(8), 1132–1135 (1992).
20. A. Boca, R. Miller, K. M. Birnbaum, *et al.*, "Observation of the vacuum Rabi spectrum for one trapped atom," Phys. Rev. Lett. **93**(23), 233603 (2004).
21. J. Johansson, S. Saito, T. Meno, *et al.*, "Vacuum Rabi oscillations in a macroscopic superconducting qubit LC oscillator system," Phys. Rev. Lett. **96**(12), 127006 (2006).
22. M. Brune, F. Schmidt-Kaler, A. Maali, *et al.*, "Quantum Rabi oscillation: A direct test of field quantization in a cavity," Phys. Rev. Lett. **76**(11), 1800–1803 (1996).
23. P. Bertet, S. Osnaghi, P. Milman, *et al.*, "Generating and probing a two-photon Fock state with a single atom in a cavity," Phys. Rev. Lett. **88**(14), 143601 (2002).
24. A. Blais, R.-S. Huang, A. Wallraff, *et al.*, "Cavity quantum electrodynamics for superconducting electrical circuits: An architecture for quantum computation," Phys. Rev. A **69**(6), 062320 (2004).
25. J. M. Fink, M. Göppl, M. Baur, *et al.*, "Climbing the Jaynes–Cummings ladder and observing its nonlinearity in a cavity QED system," Nature **454**(7202), 315–318 (2008).
26. Lev S. Bishop, J. M. Chow, Jens Koch, *et al.*, "Nonlinear response of the vacuum Rabi resonance," Nat. Phys. **5**(2), 105–109 (2009).
27. F. Altomare, J. I. Park, K. Cicak, *et al.*, "Tripartite interactions between two phase qubits and a resonant cavity," Nat. Phys. **6**(10), 777–781 (2010).
28. F. Nissen, J. M. Fink, J. A. Mlynek, *et al.*, "Collective Suppression of Linewidths in Circuit QED," Phys. Rev. Lett. **110**(20), 203602 (2013).
29. P. Macha, G. Oelsner, J.-M. Reiner, *et al.*, "Implementation of a quantum metamaterial using superconducting qubits," Nat. Commun. **5**(1), 5146 (2014).
30. M. Feng, Y. P. Zhong, T. Liu, *et al.*, "Exploring the quantum critical behaviour in a driven Tavis–Cummings circuit," Nat. Commun. **6**(1), 7111 (2015).
31. K. Kakuyanagi, Y. Matsuzaki, C. Déprez, *et al.*, "Observation of collective coupling between an engineered ensemble of macroscopic artificial atoms and a superconducting resonator," Phys. Rev. Lett. **117**(21), 210503 (2016).
32. J. M. Fink, R. Bianchetti, M. Baur, *et al.*, "Dressed collective qubit states and the Tavis-Cummings model in circuit QED," Phys. Rev. Lett. **103**(8), 083601 (2009).
33. A. F. van Loo, A. Frdorov, K. Lalumirer, *et al.*, "Photon-mediated interactions between distant artificial atoms," Science **342**(6165), 1494–1496 (2013).
34. Z.-B. Wang, P. Khatiwada, D. Wang, *et al.*, "Coherent perfect absorption in Tavis-Cummings models," Opt. Express **30**(6), 9360 (2022).